THE BELL SYSTEM
TECHNICAL JOURNAL

DEVOTED TO THE SCIENTIFIC AND ENGINEERING
ASPECTS OF ELECTRICAL COMMUNICATION

Volume 51 November, 1972 Number 9

The Static Stability of Half-Bubbles

By W. J. DeBONTE

(Manuscript received May 16, 1972)

A variational model is used to calculate the static stability limits and equilibrium properties of "half-bubbles," magnetic domains residing on one surface of a magnetic bubble material platelet. Stability is achieved through the presence of gradients in the domain wall energy density and/or saturation magnetic moment. The model evidences two distinct types of instability behavior separated by a critical value of the wall energy density gradient. Unlike the standard cylindrical domain, the half-bubble has a minimum stable value of the ratio of domain diameter to height.

The half-bubble is shown to possess a number of properties which make it potentially useful for device applications. It is self-biased by its closure wall and in some cases is stable in zero external bias. Bias margins are of the same order as those for the standard cylindrical domain. It stabilizes on only one platelet surface, and its properties are independent of both material thickness and of minor irregularities on the second surface. In addition, its structure may be advantageous in avoiding the undesirable properties of hard bubbles.

I. INTRODUCTION

The current interest in cylindrical magnetic domains and their device applications has stimulated the search for such domains in a wide variety of materials produced by a number of growth techniques. In

some samples, Bobeck[1] has observed domains of reversed magnetization which apparently do not penetrate through the entire thickness of the sample (Fig. 1). These domains, referred to as "half-bubbles," have four features which make them potentially attractive for device applications. First, they contact only one surface of the platelet in which they reside so that their properties should not be as critically dependent on surface preparation as those of the usual cylindrical domains. Second, as shown in this paper, their properties are independent of platelet thickness. Third, this article also shows that their top closure wall produces a self-biasing effect which makes external biasing unnecessary in some cases. Finally, Bobeck et al.[2] have observed in two-layer films that domains having a closure wall do not exhibit the undesirable properties of hard bubbles, and it is a reasonable presumption that this property also pertains to half-bubbles.

Bobeck[1] has suggested that half-bubbles may be stabilized by the presence of gradients normal to the material surface in one or more of the material characteristics (e.g., domain wall energy density σ_w and/or saturation magnetic moment M_s). In this paper we use a variational model to analyze the static stability of half-bubbles in materials having such gradients. Our model for the half-bubble and its instability modes is introduced in Section II. In Section III, we examine the stability of the model when the gradient in M_s is zero. While no stability occurs in this simple case, the calculation of Section III is a useful preliminary to the more general calculation of Section IV, where the gradient in M_s is assumed to be non-zero. The results of the stability calculations and their interpretation are discussed in Section V.

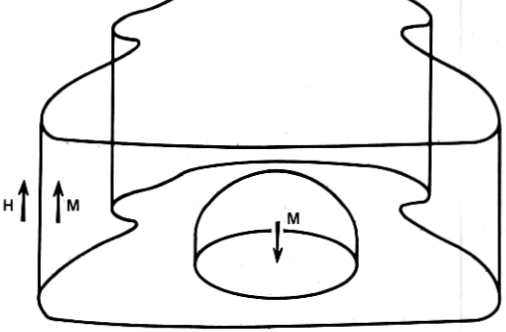

Fig. 1—Half-bubble magnetic domain configuration.

II. HALF-BUBBLE MODEL

In constructing our model we idealize the half-bubble in two ways. First, since the details of the shape of the half-bubble are not known, we approximate the actual shape of the domain by a right circular cylinder of radius r_o and height h (h assumed to be less than the platelet thickness), as shown in Fig. 2. This approximation gives the model domain a form identical to that of the standard cylindrical domain, the stability of which has been calculated by Thiele.[3] We shall exploit this identity in calculating the half-bubble energy and its derivatives. Second, we defer all consideration of the microscopic structure of the domain wall of the half-bubble and assume that the wall energy density σ_w varies linearly with distance through the platelet.

The magnetostatic energy of our half-bubble model possesses an important invariance property. As we show in Appendix A for the case in which the M_s gradient is zero, the magnetostatic energy of a cylindrical domain of fixed size located on the bottom surface of a platelet is independent of the position of the top surface of the platelet. This invariance is equally valid if M_s is a function of z, or if the domain assumes a more general shape. Thus, if we conceptually move the upper platelet surface down to the top of the model half-bubble in Fig. 2, we see that the magnetostatic energy of the half-bubble is equal to that of a standard cylindrical domain of the same size.

This invariance property has two important consequences. First, in the limit where the M_s gradient is zero, it allows us to obtain the magnetostatic energy of our model half-bubble from the results of

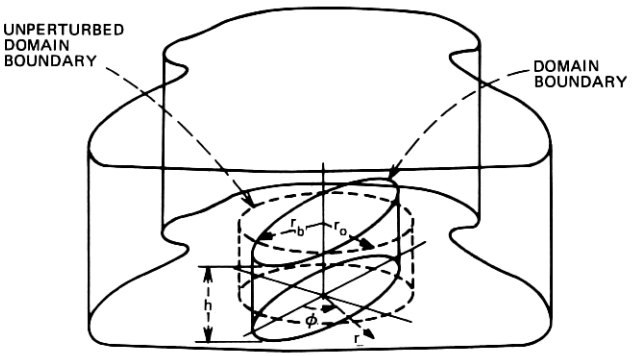

Fig. 2—Model for the half-bubble magnetic domain.

Thiele[3] and Thiele et al.[4] for the standard cylindrical domain. Second, it indicates that the platelet thickness is not a fundamental length of the half-bubble as it is for the standard cylindrical domain.

A convenient alternative standard of length, easily defined in terms of material characteristics, is provided by the material length at the bottom surface of the platelet ($z = 0$):

$$l = \sigma_w(0)/4\pi M_s^2(0). \tag{1}$$

In defining the σ_w and M_s gradient parameters γ_w and γ_M, we then scale the variations in wall energy density and saturation magnetic moment to this material length:

$$\sigma_w(z) = \sigma_w(0)\left(1 + \frac{\gamma_w z}{l}\right), \tag{2a}$$

$$M_s(z) = M_s(0)\left(1 + \frac{\gamma_M z}{l}\right). \tag{2b}$$

Experimental observation[1] indicates that there are three modes of instability which are of importance for the half-bubble: collapse, run-out, and "run-through". The general character of the collapse and run-out modes is already familiar from Thiele's stability calculation[3] for the standard cylindrical domain; the half-bubble collapse is not purely radial, however, but involves axial collapse as well. The term "run-through" is used to describe the transition from a half-bubble to a standard cylindrical domain which contacts both surfaces of the platelet.

As indicated in Fig. 2, the size of our model half-bubble is specified by the radius r_o and the height h. In considering stability against run-out, we include an elliptic distortion r_2 and specify the radial boundary of the domain by

$$r_b(\varphi) = r_o + r_2 \cos 2\varphi. \tag{3}$$

The model will be in equilibrium if the first derivatives of the total energy vanish. In the absence of in-plane anisotropy, $\partial E_T/\partial r_2 \equiv 0$ at $r_2 = 0$ by symmetry (cf. Appendix B). The equilibrium conditions are then

$$\frac{\partial E_T}{\partial r_o} = 0, \qquad \frac{\partial E_T}{\partial h} = 0. \tag{4a,b}$$

The stability of the resultant equilibrium is determined from the second derivatives, stability occurring when

$$\left(\frac{\partial^2 E_T}{\partial r_o^2}\right)_{eq.}\left(\frac{\partial^2 E_T}{\partial h^2}\right)_{eq.} - \left(\frac{\partial^2 E_T}{\partial r_o\,\partial h}\right)^2_{eq.} > 0, \tag{5}$$

$$\left(\frac{\partial^2 E_T}{\partial r_o^2}\right)_{eq.} > 0, \tag{6}$$

and

$$\left(\frac{\partial^2 E_T}{\partial r_2^2}\right)_{eq.} > 0. \tag{7}$$

If the inequality in eq. (5) is replaced by the corresponding equality, then the half-bubble is on the verge of either collapse or run-through. If $(\partial E_T/\partial r_2^2)_{eq.} = 0$, then the model is about to undergo run-out.

III. HALF-BUBBLE STABILITY WITH CONSTANT M_s

We begin the actual calculation of the stability limits for the half-bubble by considering the limiting case of constant M_s. This case lacks practical interest since we show that it leads to no region of stability for half-bubbles. In this limit, however, the problem loses much of the analytic complexity which characterizes the general case in which the gradient parameter $\gamma_M \neq 0$. Our method of solution–treating the second derivatives of the energy as polynomials in h/l with coefficients depending only on $2r_o/h$–thus becomes clearly visible here.

As noted in the preceding section, our half-bubble model is markedly similar in form to the model used by Thiele[3] and Thiele et al.[4] to treat the standard cylindrical domain. For this reason, in the present calculation we adopt the notation of these papers wherever practical.

The total energy of the half-bubble, measured relative to that of the uniformly-magnetized platelet, is

$$E_T = E_w + \Delta E_H + \Delta E_M \tag{8}$$

where E_w is the wall energy, (including the energy of the top closure wall), ΔE_H is the energy of interaction with the externally applied bias field, and ΔE_M is the magnetostatic energy. Since the half-bubble is independent of the magnetic material above it, we can describe our model in terms of the unit step function u as

$$\vec{M} = \hat{\imath}_z[1 - 2u(r_b(\varphi) - r)]u(z)u(h - z) \tag{9}$$

where $r_b(\varphi)$ is as defined in eq. (3).

The wall energy, consisting of integrals of $\sigma_w(z)$ over the side and top surfaces of the half-bubble, assumes the form

$$E_w = \int_0^h \sigma_w(z)\,dz \int_0^{2\pi} \left\{ r_b^2(\varphi) + \left(\frac{\partial r_o}{\partial \varphi}\right)^2 \right\}^{\frac{1}{2}} d\varphi + \sigma_w(h) \int_0^{2\pi} \frac{r_b^2(\varphi)}{2}\,d\varphi. \tag{10}$$

From eq. (10) it is clear that different wall energy densities for side and top walls could easily be included in our model. While such a distinction has intuitive appeal, experimental evidence on this point is lacking. We thus omit this added degree of freedom in the present calculation.

The energy of interaction with the external bias field $\vec{H} = \hat{\imath}_z H$, relative to that for the uniformly magnetized plate, is

$$\Delta E_H = -2 \int_{\text{h.}-\text{b.}} \vec{M}\cdot\vec{H}\,dV = M_s H h \int_0^{2\pi} r_b^2(\varphi)\,d\varphi. \tag{11}$$

If the elliptical distortion r_2 is set equal to zero, E_w and ΔE_H become

$$E_w = 2\pi r_o h \sigma_w(0)\left(1 + \frac{\gamma_w h}{2l}\right) + \pi r_o^2 \sigma_w(0)\left(1 + \frac{\gamma_w h}{l}\right) \tag{12a}$$

$$= 2\pi r_o h \sigma_w(h/2) + \pi r_o^2 \sigma_w(h), \tag{12b}$$

$$\Delta E_H = 2\pi r_o^2 h M_s H. \tag{13}$$

It should be noted that the interaction energy ΔE_H is proportional to the domain volume $\pi r_o^2 h$. This characteristic is shared by the gradient term in the energy of the top wall [eq. (12)], leading us to view this term as arising from an effective bias field. The non-gradient part of the top wall energy lacks any h-dependence, being proportional to πr_o^2. It may be thought of as coming from an h-dependent bias field analogous to that introduced by Liu[5] in connection with sputtered thin films which are exchange-coupled to a magnetic bubble material.

The relative magnetostatic energy is obtained from the general expression

$$E_M = \frac{1}{2} \int_v dV \int_{v'} dV' \frac{(\nabla\cdot\vec{M})(\nabla'\cdot\vec{M}')}{|\vec{r} - \vec{r}'|} \tag{14}$$

in the form

$$\Delta E_M = M_s^2 \int_0^\infty r\,dr \int_0^{2\pi} d\varphi \int_0^\infty r'\,dr' \cdot \int_0^{2\pi} d\varphi' [kk' - 1][\rho^{-1} - (\rho^2 + h^2)^{-\frac{1}{2}}] \tag{15}$$

where

$$k(r, r_b(\varphi)) = 1 - 2u(r_b(\varphi) - r), \tag{16}$$

$$\rho^2 = r^2 + r'^2 - 2rr' \cos(\varphi - \varphi'). \tag{17}$$

This integral is given in closed form by Thiele et al.[3] for the case $r_2 = 0$:

$$\Delta E_M = -2\pi h^3 \cdot 2\pi M_s^2 I(x), \tag{18}$$

$$I(x) = -\frac{2x}{3\pi}\left\{x^2 + \left(1 + \frac{1}{x^2}\right)^{\frac{1}{2}}\left[(1 - x^2)E\left(\frac{x^2}{1 - x^2}\right) - K\left(\frac{x^2}{1 - x^2}\right)\right]\right\} \tag{19}$$

where $x = 2r_o/h$ and K, E are complete elliptic integrals.

It is now a straightforward matter to differentiate E_T with respect to r_o, h, and r_2. Using the definitions for the normalized bias field $\tilde{H}$ and Thiele's[3] wall-force function F

$$\tilde{H} = H/4\pi M_s, \tag{20}$$

$$F(x) \equiv \frac{dI(x)}{dx} = \frac{2x^2}{\pi}\left[\left(1 + \frac{1}{x^2}\right)^{\frac{1}{2}}E\left(\frac{x^2}{1 - x^2}\right) - 1\right], \tag{21}$$

we may conveniently write the equilibrium conditions $\partial E_T/\partial r_o = 0$, $\partial E_T/\partial h = 0$ in normalized form as

$$\frac{l}{h}\left(1 + \frac{\gamma_w h}{2l}\right) + \frac{1}{2}x\frac{l}{h}\left(1 + \frac{\gamma_w h}{l}\right) + x\tilde{H} - F(x) = 0, \tag{22a}$$

$$\frac{l}{h}\left(1 + \frac{\gamma_w h}{l}\right) + \tfrac{1}{4}x\gamma_w + \tfrac{1}{2}x\tilde{H} - \frac{3}{x}I(x) + F(x) = 0. \tag{22b}$$

To show the biasing effect of the top wall we write eq. (22a) as

$$\frac{l(h/2)}{h} + x\left[\tilde{H} + \frac{1}{2}\frac{l(h)}{h}\right] - F(x) = 0 \tag{23}$$

where $l(h/2)$ and $l(h)$ are the material lengths as measured at the middle and at the top of the domain, respectively, and are defined by the obvious generalization of eq. (1). Equation (23) should be compared with the force equation for the standard cylindrical domain [Ref. 2, eq. (69)]

$$\frac{l}{h} + x\tilde{H} - F(x) = 0. \tag{24}$$

Equations (22a) and (22b) may also be used to obtain expressions for the values of γ_w and $\tilde{H}$ required to obtain an equilibrium state characterized by specified values of l/h and x:

$$\gamma_w = -\frac{2}{3}\frac{l}{h}\left(1 - \frac{x}{2}\right) + \frac{4}{x}I(x) - 2F(x) \tag{25a}$$

$$\tilde{H} = -\frac{1}{3}\frac{l}{h}\left(\frac{2}{x} + 1 + \frac{x}{2}\right) - 2\left(\frac{1}{x} + \frac{1}{x^2}\right)I(x) + \left(1 + \frac{2}{x}\right)F(x). \quad (25b)$$

The stability or instability of a given equilibrium point is determined by examining the second derivatives of the energy. Calculating these derivatives and removing a factor of $\beta^{-1} = 4\pi h \cdot 4\pi M_s^2$ we find

$$\beta \frac{\partial^2 E_T}{\partial r_o^2} = \frac{1}{2}\frac{l}{h} + \tfrac{1}{2}\gamma_w + \tilde{H} - \frac{dF(x)}{dx}, \quad (26a)$$

$$\beta \frac{\partial^2 E_T}{\partial h\, \partial r_o} = \frac{1}{2}\frac{l}{h} + \frac{1}{2}\gamma_w\left(1 + \frac{x}{2}\right) + \frac{1}{2}x\tilde{H} - F(x) + \frac{x}{2}\frac{dF(x)}{dx}, \quad (26b)$$

$$\beta \frac{\partial^2 E_T}{\partial h^2} = \frac{1}{4}x\gamma_w - \frac{3}{2}I(x) + xF(x) - \frac{x^2}{4}\frac{dF(x)}{dx}, \quad (26c)$$

$$\beta \frac{\partial^2 E_T}{\partial r_2^2} = \frac{l}{h}\left(\frac{1}{4} + \frac{2}{x}\right) + \gamma_w\left(\frac{1}{4} + \frac{1}{x}\right) + \frac{1}{2}\tilde{H} - \frac{4}{x^2}I(x) + \frac{2}{x}F(x) - \frac{1}{2}\frac{dF(x)}{dx}. \quad (26d)$$

Operations with these second derivatives are simplified if we define

$$G(x) \equiv -I(x) + xF(x) - \frac{x^2}{2}\frac{dF(x)}{dx}. \quad (27)$$

Using the relation[6]

$$\frac{2}{x}I(x) - F(x) = \tfrac{1}{4}(S_o(x) + 3S_2(x)) \quad (28)$$

we may write $G(x)$ in terms of the stability functions $S_o(x)$ and $S_2(x)$ of Ref. 3:

$$G(x) = \tfrac{3}{8}x(S_o(x) - S_2(x)). \quad (29)$$

After consulting plots[3] of $S_o(x)$ and $S_2(x)$, it is easily seen that $G(x) \geqq 0$ for $x \geqq 0$.

If we use eqs. (25a, b) to eliminate γ_w, $\tilde{H}$ from eqs. (26a–d), we obtain expressions for the second derivatives of E_T at equilibrium in terms of l/h and x only

$$\beta\left(\frac{\partial^2 E_T}{\partial r_o^2}\right)_{eq.} = -\frac{1}{3}\frac{l}{h}\left(\frac{2}{x} + \frac{1}{2}\right) + \frac{2}{x^2}G(x), \quad (30a)$$

$$\beta\left(\frac{\partial^2 E_T}{\partial h\, \partial r_o}\right)_{eq.} = -\frac{1}{6}\frac{l}{h}(1 + x) - \frac{1}{x}G(x), \quad (30b)$$

$$\beta\left(\frac{\partial^2 E_T}{\partial h^2}\right)_{eq.} = -\frac{1}{6}\frac{l}{h}x\left(1 - \frac{x}{2}\right) + \frac{1}{2}G(x), \quad (30c)$$

$$\beta\left(\frac{\partial^2 E_T}{\partial r_2^2}\right)_{eq.} = \frac{l}{h}\left(\frac{1}{4}+\frac{1}{x}\right)+\frac{1}{x^2}G(x). \tag{30d}$$

The derivatives are now in a form suitable for comparison with the stability conditions, eqs. (5–7). Inspection of eq. (30d) shows that $\beta(\partial^2 E_T/\partial r_2^2)_{eq.} > 0$ for all positive values of l/h so that eq. (7) is satisfied for this system. Equation (6) is satisfied if

$$\frac{l}{h} < \frac{6}{x^2}G(x)\left(\frac{2}{x}+\frac{1}{2}\right)^{-1}. \tag{31}$$

Finally, we require

$$\beta^2\left[\left(\frac{\partial^2 E_T}{\partial r_o^2}\right)_{eq.}\left(\frac{\partial^2 E_T}{\partial h^2}\right)_{eq.} - \left(\frac{\partial^2 E_T}{\partial r_o\,\partial h}\right)^2_{eq.}\right]$$
$$= \frac{1}{12}\left(\frac{l}{h}\right)^2\left(1-x-\frac{x^2}{2}\right)-\frac{l}{h}\left(\frac{1}{x}+\frac{1}{4}\right)G(x) > 0 \tag{32}$$

which may be factored[7] into $l/h > 0$ and

$$\frac{l}{h} > \left(\frac{12}{x}+3\right)G(x)\left(1-x-\frac{x^2}{2}\right)^{-1}. \tag{33}$$

However, it is easy to show that eqs. (31), (33) and the condition $l/h > 0$ cannot be simultaneously satisfied. Thus, if $\gamma_M = 0$, the half-bubble model has no stability against collapse and/or run-through.

While its result is negative, this stability calculation illustrates the method used in this paper for separating the l/h- and d/h-dependence of the half-bubble model and for finding its stability region. We first use the equilibrium conditions to remove γ_w and $\tilde{H}$ from the expressions for the second derivatives of E_T. The resultant expressions are essentially polynomials in l/h with coefficients depending only upon $x = d/h$ [cf. the right-hand sides of eqs. (30a–d) and (32)]. For fixed x, the roots of these polynomials provide us with the limits of the stability region (if one exists). In the next section, we generalize this method to include the effects of non-zero γ_M.

IV. HALF-BUBBLE STABILITY WITH $\gamma_M \neq 0$

We now generalize the equations of Section III to calculate the stability of the half-bubble model in the presence of a gradient in the saturation moment M_s. The wall energy E_w is unchanged from the expression given in eq. (10) and the interaction energy ΔE_H only gains a new factor to become

$$\Delta E_H = M_s\left(1 + \frac{\gamma_M h}{2l}\right)Hh \int_0^{2\pi} r_b^2(\varphi)\, d\varphi. \tag{34}$$

The expressions for the magnetostatic energy, however, become substantially more complex than those given in eqs. (15) through (19).

The magnetization distribution of eq. (9) is now replaced by

$$\vec{M} = \hat{\imath}_z M_s(0)\left(1 + \frac{\gamma_M z}{l}\right)[1 - 2u(r_b(\varphi) - r)]u(z)u(h - z). \tag{35}$$

The corresponding magnetostatic charge density is

$$-\nabla\cdot\vec{M} = -M_s(0)[1 - 2u(r_b(\varphi) - r)] \times \left\{\delta(z) - \delta(z - h) + \frac{\gamma_M h}{l}\left[-\delta(z - h) + \frac{1}{h}u(z)u(h - z)\right]\right\}. \tag{36}$$

The first two δ-functions in this expression are the familiar platelet surface charge terms which occur in the stability theory of the standard cylindrical domain [Ref. 3, eq. (19)]. The third δ-function gives the correction to the charge on the upper surface, while the product of step-functions describes the uniform volume charge resulting from the gradient γ_M.

The magnetostatic energy integral of eq. (14) has a quadratic dependence on the charge density $-\nabla\cdot\vec{M}$. As a result, we have terms in ΔE_M up to second order in γ_M. For convenience, we write

$$\Delta E_M = E_M^{(0)} + \gamma_M E_M^{(1)} + \gamma_M^2 E_M^{(2)} \tag{37}$$

where $E_M^{(0)}$ is identical to the magnetostatic energy of the preceding section. The quantity $\gamma_M E_M^{(1)}$ has two parts. The first arises from the interaction of the $\gamma_M = 0$ charge distribution with the uniform volume charge and is zero by symmetry. The second, representing the interaction of the $\gamma_M = 0$ charge distribution with the excess charge on the upper surface, is easily evaluated. We find

$$\gamma_M E_M^{(1)} = \frac{\gamma_M h}{l} E_M^{(0)}. \tag{38}$$

The final term $\gamma_M^2 E_M^{(2)}$ may be written as

$$\gamma_M^2 E_M^{(2)} = \frac{1}{2}\left(\frac{\gamma_M h}{l}\right)^2 M_s^2(0) \int_0^\infty r\, dr \int_0^{2\pi} d\varphi \int_0^\infty r'\, dr' \int_0^{2\pi} d\varphi'(kk' - 1) \times \left\{\rho^{-1} - 2h^{-1}\int_0^h dz[\rho^2 + (z - h)^2]^{\frac{1}{2}} + h^{-2}\int_0^h dz \int_0^h dz'[\rho^2 + (z - z')^2]^{\frac{1}{2}}\right\}. \tag{39}$$

The ρ^{-1} term in the curly brackets corresponds to the self-energy of the excess charge on the upper platelet surface; the z-integral following it arises from the interaction of this excess charge with the uniform volume

charge, and the double-z-integral corresponds to the self-energy of the volume charge. After evaluating the z-integrals, we obtain the following integral expression for the second-order energy:

$$\gamma_M^2 E_M^{(2)} = \left(\frac{\gamma_M h}{l}\right)^2 M_s^2(0) \int_0^\infty r\,dr \int_0^{2\pi} d\varphi \int_0^\infty r'\,dr' \int_0^{2\pi} d\varphi'(kk' - 1) \times \left\{2\rho^{-1} - \frac{\rho - (\rho^2 + h^2)^{\frac{1}{2}}}{h^2}\right\}. \tag{40}$$

Setting $r_2 = 0$, we find

$$\gamma_M^2 E_M^{(2)} = \frac{1}{15}\left(\frac{\gamma_M h}{l}\right)^2 (2\pi M_s^2(0))(2\pi h^3) \cdot \left\{\frac{x^3}{\pi} - (x + x^3)F(x) - (3 - x^2)I(x)\right\}. \tag{41}$$

The derivatives of the total energy E_T are now used to find the range of stability of the half-bubble model. Experimentally, this stable range would be mapped out by selecting materials characterized by given values of γ_w and γ_M and then varying $\tilde{H}$ to find the stable region in the variables d/l and h/l. The analytic form of our equations, however, precludes following such a physical approach in the present calculation. Instead, we use an extension of the method followed in Section III. We use the equilibrium conditions eqs. (4a, b) to eliminate γ_w and $\tilde{H}$ from the second derivatives and then treat the second derivatives as polynomials in $y \equiv h/l$, the coefficients of the polynomials being functions of $x \equiv d/h$ and γ_M. This manifestly unphysical approach gives the desired stable regions with a minimum of algebraic and numerical complexity.

The equilibrium conditions corresponding to eqs. (4a, b) are conveniently written in the following normalized forms:

$$\frac{l}{h}\left(1 + \frac{x}{2}\right) + \frac{\gamma_w}{2}(1 + x) + x\tilde{H}\left(1 + \frac{\gamma_M h}{2l}\right) - \left(1 + \frac{\gamma_M h}{l}\right)F(x) + \frac{1}{3}\left(\frac{\gamma_M h}{l}\right)^2\left[\frac{x^2}{\pi} - (1 + x^2)F(x) + xI(x)\right] = 0, \tag{42a}$$

$$\frac{l}{h} + \gamma_w\left(1 + \frac{x}{4}\right) + \frac{1}{2}x\tilde{H}\left(1 + \frac{\gamma_M h}{l}\right) + F(x) - \frac{3}{x}I(x) + \frac{\gamma_M h}{l}\left[F(x) - \frac{4}{x}I(x)\right] - \left(\frac{\gamma_M h}{l}\right)^2 \frac{1}{x}I(x) = 0. \tag{42b}$$

These equations may be solved to find the appropriate values of γ_w and $\tilde{H}$ for an equilibrium state characterized by given values of γ_M, x, and $y \equiv h/l$. For brevity we write $F(x)$ and $I(x)$ as F and I respectively, and define a denominator D by

$$D = y\left[3 + \gamma_M\left(1 - \frac{x}{2}\right)y\right]. \tag{43}$$

We then find

$$\gamma_w = D^{-1}\Big\{(x-2) + (\gamma_M x - 6F + 12x^{-1}I)y + \gamma_M(-10F + 22x^{-1}I)y^2 + \frac{2}{3}\gamma_M^2\left[\frac{x^2}{\pi} - (7+x^2)F + \left(\frac{18}{x} + x\right)I\right]y^3 + \frac{2}{3}\gamma_M^3\left[\frac{x^2}{\pi} - (1+x^2)F + \left(\frac{3}{x} + x\right)I\right]y^4\Big\}, \tag{44a}$$

$$\tilde{H} = D^{-1}\Big\{-\left(\frac{2}{x} + 1 + \frac{x}{2}\right) + \left[\left(\frac{6}{x} + 3\right)F - \left(\frac{6}{x^2} + \frac{6}{x}\right)I\right]y + \gamma_M\left[\left(\frac{6}{x} + 3\right)F - \left(\frac{8}{x^2} + \frac{8}{x}\right)I\right]y^2 - \gamma_M^2\left[\frac{1}{3}\left(\frac{4}{x} + 1\right)\left(\frac{x^2}{\pi} - (1+x^2)F + xI\right) + \frac{2}{x^2}(1+x)I\right]y^3\Big\}. \tag{44b}$$

The denominator D in both of these expressions is always greater than zero and finite in the region of interest, and thus contributes no singularities or zeros to the calculation.

The second derivatives of E_T are developed in much the same fashion as in Section III. They are cast in dimensionless form by extracting a factor of $\beta^{-1} = 4\pi h \cdot 4\pi M_s^2(0)$, and γ_w and $\tilde{H}$ are then eliminated using eqs. (44a, b). The resultant expressions assume the form of polynomials in y after being multiplied by D. Because of the length of the expressions, we give only the final polynomial forms:

$$D\beta\left(\frac{\partial^2 E_T}{\partial r_o^2}\right)_{\text{eq.}} = -\left(\frac{2}{x} + \frac{1}{2}\right) + \left(\frac{6}{x^2}G - \frac{\gamma_M}{x}\right)y - \gamma_M\left[\left(4 - \frac{x}{2}\right)\frac{dF}{dx} - \left(\frac{9}{x} - \frac{1}{2}\right)F + \frac{11}{x^2}I\right]y^2 + \gamma_M^2\left[\frac{2}{3}\frac{x}{\pi} - \left(2 - \frac{x}{2} + x^2\right)\frac{dF}{dx} + \left(\frac{13}{3x} - \frac{1}{2} + \frac{x}{3}\right)F - \left(\frac{6}{x^2} + \frac{1}{3}\right)I\right]y^3 + \frac{\gamma_M^3}{3}\left[-\frac{x^2}{2\pi} + \left(\frac{x}{2} - 1\right)(x^2+1)\frac{dF}{dx} + \left(\frac{2}{x} - \frac{1}{2} + x\right)F - \left(\frac{3}{x^2} + 1\right)I\right]y^4 \tag{45a}$$

$$D\beta\left(\frac{\partial^2 E_T}{\partial r_o\, dh}\right)_{eq.} = -\frac{1}{2}(1+x) - \left[\frac{3}{x}G + \frac{\gamma_M}{2}\left(1+\frac{x}{2}\right)\right]y$$
$$+ \gamma_M\left[\frac{x}{2}\left(4-\frac{x}{2}\right)\frac{dF}{dx} - \left(\frac{9}{2}-x\right)F + \left(\frac{4}{x}-\frac{3}{2}\right)I\right]y^2$$
$$+ \gamma_M^2\left[-\frac{x^2}{3\pi} + \frac{x}{2}\left(1-\frac{x}{2}\right)\frac{dF}{dx}\right.$$
$$\left. - \left(\frac{5}{3}-\frac{5x}{4}-\frac{x^2}{3}\right)F + \left(\frac{1}{x}-2-\frac{x}{3}\right)I\right]y^3$$
$$+ \frac{\gamma_M^3}{3}\left[-\frac{x^2}{\pi} - \left(\frac{1}{2}-\frac{3x}{4}-x^2\right)F - \left(\frac{3}{2}+x\right)I\right]y^4 \quad (45b)$$

$$D\beta\left(\frac{\partial^2 E_T}{\partial h^2}\right)_{eq.} = -\frac{x}{2}\left(1-\frac{x}{2}\right) + \left[\frac{3}{2}G - \frac{\gamma_M x}{4}\left(1-\frac{x}{2}+\frac{x^2}{4}\right)\right]y$$
$$+ \gamma_M\left[-x^2\left(1-\frac{x}{8}\right)\frac{dF}{dx} + \left(\frac{15}{4}x - \frac{x^2}{8}\right)F - \frac{23}{4}I\right]y^2$$
$$+ \gamma_M^2\left[\frac{x^3}{6\pi} - \frac{x^2}{4}\left(1-\frac{x}{2}\right)\frac{dF}{dx}\right.$$
$$\left. + \left(\frac{11x}{6}-\frac{3x^2}{8}-\frac{x^3}{6}\right)F - \left(4-\frac{x}{2}-\frac{x^2}{6}\right)I\right]y^3$$
$$+ \frac{\gamma_M^3}{12}\left[-\frac{x^4}{2\pi} + \left(3x-x^2+\frac{x^4}{2}\right)F - \left(9-3x+\frac{x^3}{2}\right)I\right]y^4 \quad (45c)$$

$$D\beta\left(\frac{\partial^2 E_T}{\partial r_2^2}\right)_{eq.} = \left(\frac{3}{x}+\frac{3}{4}\right) + \left[\frac{3}{x^2}G + \frac{3\gamma_M}{2x}\right]y$$
$$+ \gamma_M\left[-\left(2-\frac{x}{4}\right)\frac{dF}{dx} + \frac{5}{4}\left(\frac{2}{x}-1\right)F + \left(\frac{1}{2x^2}+\frac{2}{x}\right)I\right]y^2$$
$$+ \gamma_M^2\left[-\frac{x}{5\pi} - \left(1-\frac{x}{4}+\frac{x^2}{2}\right)\frac{dF}{dx}\right.$$
$$\left. + \left(\frac{7}{10x}-\frac{5}{4}+\frac{7x}{10}\right)F + \left(\frac{13}{5x^2}+\frac{2}{x}-\frac{7}{10}\right)I\right]y^3$$
$$+ \gamma_M^3\left[(16+7x)\frac{x}{60\pi} - \frac{1}{6}\left(1-\frac{x}{2}+x^2-\frac{x^3}{2}\right)\frac{dF}{dx}\right.$$
$$\left. + \frac{1}{5}\left(\frac{1}{3x}+\frac{17}{12}-\frac{x}{2}-x^2\right)F + \frac{1}{5}\left(\frac{7}{2x^2}+\frac{2}{x}+\frac{1}{2}+x\right)I\right]y^4 \quad (45d)$$

The problem of finding the ranges of parameters yielding stability of the half-bubble model now becomes one of numerical analysis. For given values of x and γ_M we find the zeros of the three polynomials

$$D^2\beta^2\left[\left(\frac{\partial^2 E_T}{\partial r_o^2}\right)_{eq.}\left(\frac{\partial^2 E_T}{\partial h^2}\right)_{eq.} - \left(\frac{\partial^2 E_T}{\partial r_o\,\partial h}\right)^2_{eq.}\right],$$

$$D\beta\left(\frac{\partial^2 E_T}{\partial r_o^2}\right)_{eq.}, \quad \text{and} \quad D\beta\left(\frac{\partial^2 E_T}{\partial r_2^2}\right)_{eq.}.$$

A stable region corresponds to a range of y beginning and ending with one of these zeros and having the property that all three of the polynomials are positive for values of y on the interior of the interval.

The results of this procedure are shown for $\gamma_M = -0.025$, -0.05, and -0.1 in Figs. 3–5. The stable regions are plotted in the x, $1/y$ plane; $1/y = l/h$ was used as a coordinate in order to facilitate comparison with the results of Thiele for the standard cylindrical domain (cf. Ref. 3, Fig. 3). In the interior of the stable region we have provided two families of curves which describe the behavior of a stable half-bubble. The families γ_w = constant and $\tilde{H}$ = constant are obtained from the polynomials of eqs. (44a, b) after the boundaries of the stability region have been found. Since h is not fixed in the half-bubble, the domains do not follow lines of l/h = constant as $\tilde{H}$ is varied. Rather, they follow the curves γ_w = constant which characterize the given material.

V. DISCUSSION

We have explored the static stability of the half-bubble magnetic domain using a variational model. In spite of the simplicity of our model, the generality of some of the principles underlying our calculation lead us to expect that our results have at least semi-quantitative validity (cf. Appendices A and B).

Typical results of our stability calculation are shown in Figs. 3–5. The boundaries of each of the half-bubble stability regions shown in the figures roughly resemble two connected parabolic line segments, both parabolas opening to the right. The lower segment is determined by the zeros of the polynomial $D\beta(\partial^2 E_T/\partial r_2^2)_{eq.}$ and corresponds to the run-out instability mode. The upper segment arises from the zeros of

$$D^2\beta^2\left[\left(\frac{\partial^2 E_T}{\partial r_o^2}\right)_{eq.}\left(\frac{\partial^2 E_T}{\partial h^2}\right)_{eq.} - \left(\frac{\partial^2 E_T}{\partial r_o\,\partial h}\right)^2_{eq.}\right].$$

This part of the boundary gives the limits of stability against run-through and collapse. Thus, the lines γ_w = constant on the right side

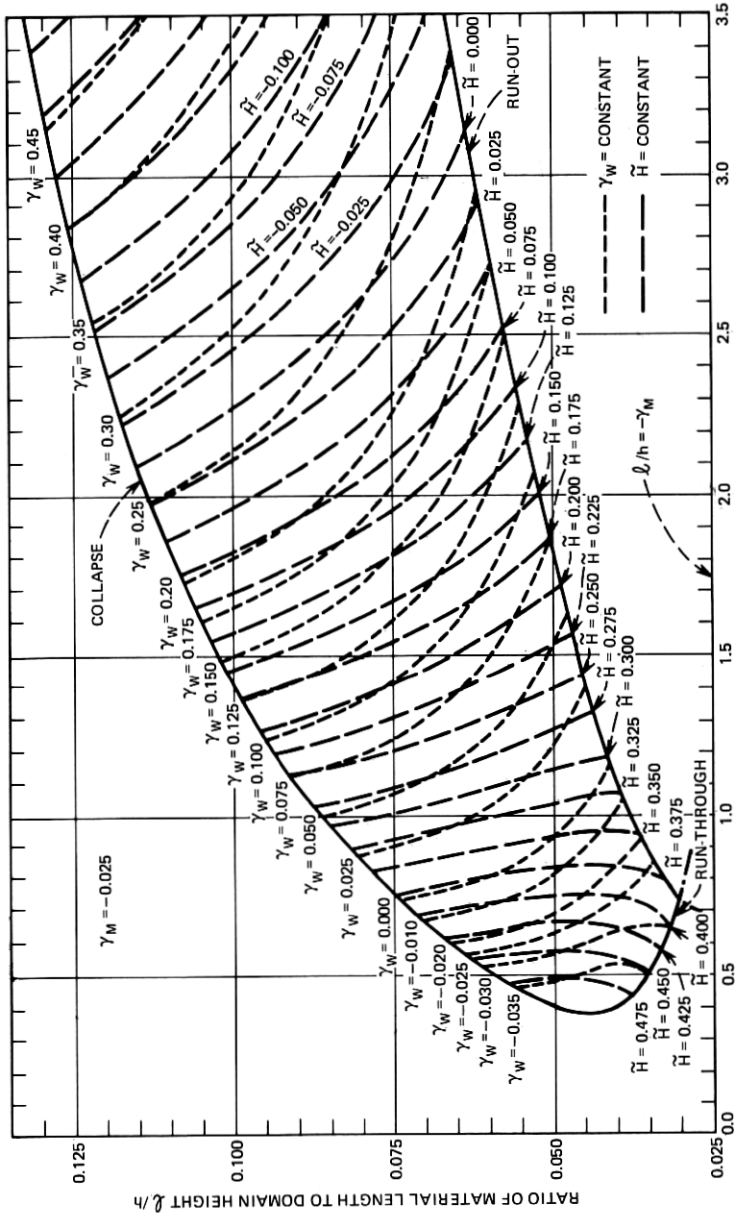

Fig. 3—Static stability chart for the half-bubble model, $\gamma_M = -0.025$.

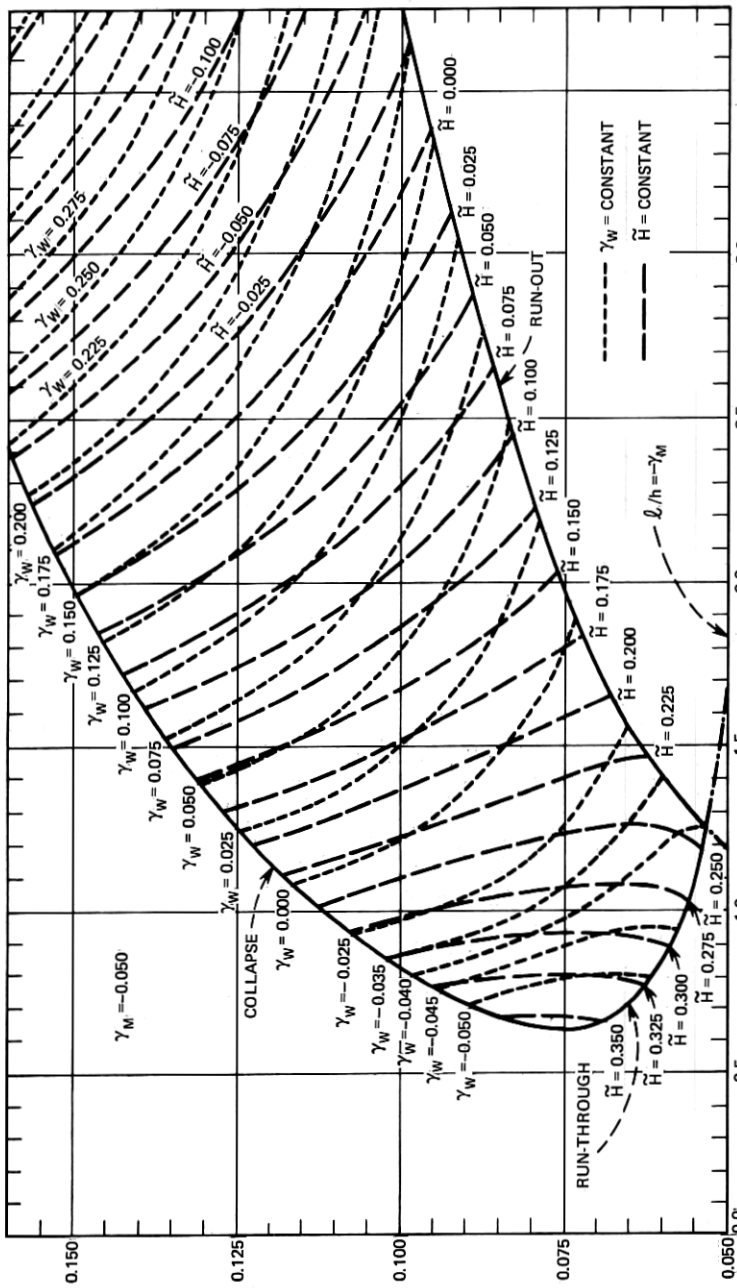

Fig. 4—Static stability chart for the half-bubble model, $\gamma_M = -0.050$.

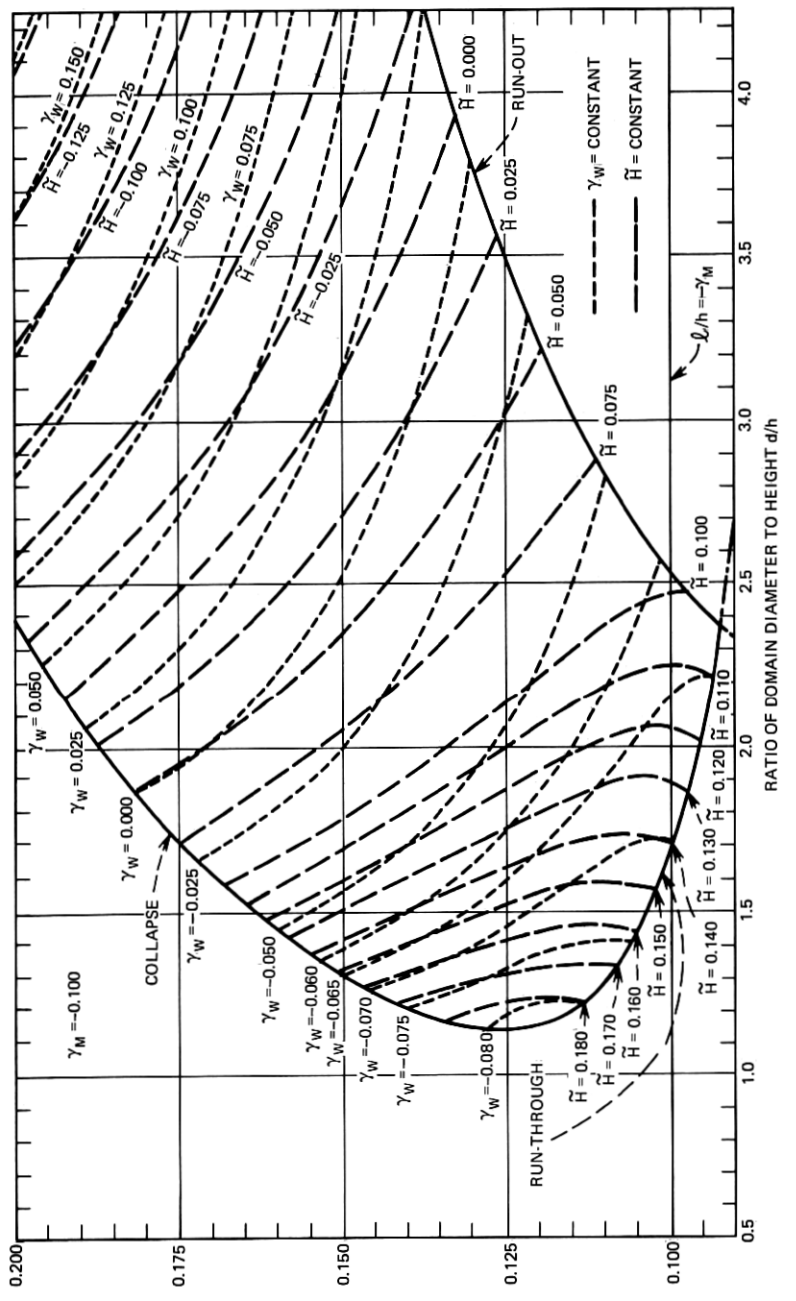

Fig. 5—Static stability chart for the half-bubble model, $\gamma_M = -0.100$.

of the figure go from run-out at the low-$\tilde{H}$ end of the line to collapse on the high-$\tilde{H}$ end. Values of γ_w which are algebraically small enough to correspond to lines on the left end of the stable region follow a different pattern, going from collapse to run-through as $\tilde{H}$ is decreased. Our stability charts then indicate two fundamentally different types of behavior as $\tilde{H}$ is decreased: the half-bubbles may undergo run-through to assume the shape of a standard cylindrical domain (and then presumably run out as $\tilde{H}$ is decreased further),[8] or the half-bubble may run out first (presumably to undergo run-through as $\tilde{H}$ is further lowered and give the usual demagnetized stripe pattern). These two types of behavior are separated by a critical wall energy gradient γ_{wc} which is a function of γ_M, being approximately -0.027 and -0.04 for $\gamma_M = -0.025$ and -0.050, respectively. (For $\gamma_M = -0.1$, the problem is more complicated and will be discussed below.)

Comparison of the half-bubble stability regions with those of the standard cylindrical domain (Ref. 3, Fig. 3) reveals one marked difference between the two systems. In the half-bubble case, there is a minimum stable value of d/h for given γ_M. For $\gamma_M = -0.025$, -0.050, and -0.100, these minimum values are $d/h = 0.39$, 0.64, and 1.14, respectively. Long, narrow bubbles are then not attainable in the half-bubble system.

It should be noted that all three of the stability charts correspond to $\gamma_M < 0$. While a general proof of the instability of half-bubbles with positive γ_M has not been formulated, numerical investigations show no regions of stability for $\gamma_M > 0$. As was shown to be the case for $\gamma_M = 0$, eqs. (5) and (6) could not be satisfied simultaneously for $\gamma_M > 0$. This property of gradient-stabilized half-bubbles is actually an advantage for device work as it implies a useful type of stability. A half-bubble originating on the lower surface of a platelet, after being allowed to undergo run-through, cannot be squeezed down to a half-bubble residing on the upper surface as $\tilde{H}$ is increased again. The domain is thus forced to return to its original state, the half-bubble state on the opposite surface being unstable.

In addition to the stability limits imposed by the derivatives of the energy function E_T, we place a lower limit on l/h by requiring $\sigma_w(h) > 0$ and $M_s(h) > 0$. While the motivation for the restriction $\sigma_w(h) > 0$ is physically obvious, the reason for the requirement $M_s(h) > 0$ stems more from the limitations of our model than from physical considerations. Magnetic materials may be compensated so that $M_s(z)$ goes linearly with z from positive to negative values. In the presence of a bias field, however, the magnetization in such a material would be aligned so that

its variation could no longer be described in terms of a linear variation with z. Such a compensated material would then not be susceptible to the present analysis and would presumably give rise to domains with different characteristics than those considered here. Taken together, the conditions $\sigma_w(h) > 0$ and $M_s(h) > 0$ yield the restriction

$$l/h > \max(-\gamma_w, -\gamma_M). \tag{46}$$

In practice, it may be necessary to require that l/h be even greater than the lower limit implied by eq. (46) since $\sigma_w(z) > 0$ must be satisfied not only at the top of the half-bubble ($z = h$), but throughout the region of the platelet above the half-bubble ($z > h$). (By a simple extension of Appendix A, we need not require $M_s(z) > 0$ in the region above the half-bubble.) These restrictions indicate that our calculation is not valid for part of the lower end of the stability region obtained for $\gamma_M = -0.100$ (cf. Fig. 5). As a consequence, the critical wall energy gradient γ_{wc} discussed above cannot be defined in this case.

The normalized bias fields $\tilde{H}$ required to stabilize half-bubbles are somewhat smaller than those needed for standard cylindrical domains as a result of the self-biasing effect provided by the upper closure wall (cf. Section III). Without going to unreasonably large values of γ_w, cases are found which are stable with $\tilde{H} = 0$ or even $\tilde{H} < 0$ ($\vec{H}$ parallel to the magnetization inside the domain). In addition, bias margins for the half-bubble are of the order of those for the standard cylindrical domain, typically falling in the range $0.04 \lesssim \Delta\tilde{H} \lesssim 0.08$. Thus if $4\pi M_s(o)$ is 200 gauss, bias field margins will be of the order 8 to 16 gauss.

To demonstrate the use of the stability charts in obtaining numerical information, we consider the case $\gamma_M = -0.100$ and $\gamma_w = +0.025$, for which a half-bubble is stable in zero bias field. The variations in σ_w and M_s between the bottom and the top of the half-bubble are easily computed after obtaining a value of l/h from the stability chart. In the present case, $l/h = 0.152$ corresponds to zero bias. Evaluating $\gamma_w h/l$ and $\gamma_M h/l$, we find that σ_w increases by 16.4 percent and M_s decreases by 65.8 percent between the bottom and the top of the half-bubble.

The collapse and run-out fields for $\gamma_M = -0.100$ and $\gamma_w = 0.025$ are found by interpolating between the $\tilde{H}$ = constant curves in Fig. 5. We find $\tilde{H}_{\text{coll.}} \cong 0.017$ and $\tilde{H}_{\text{run.}} \cong -0.023$ giving a bias margin of $\Delta\tilde{H} = 0.040$. The size variations of the half-bubble over its stable range are best measured in terms of the $z = 0$ material length defined by eq. (1). For any operating point in the stable range, $h/l = (l/h)^{-1}$ can be found from the vertical coordinate of the point while $d/l = (d/h)(l/h)^{-1}$ can be found as the ratio of the horizontal and vertical coordinates. For

$\gamma_M = -0.100$ and $\gamma_w = +0.025$ we find $(h/l)_{\text{coll.}} = 5.38$, $(d/l)_{\text{coll.}} = 10.85$, $(h/l)_{\text{run.}} = 7.27$, and $(d/l)_{\text{run.}} = 30.91$. Thus, while d increases by a factor of three between collapse and run-out, h increases by only 35 percent over this same range. Since the curves $\tilde{H}$ = constant and γ_w = constant are nearly parallel at the collapse end of the stable range, much of this change in h occurs with a very small change in $\tilde{H}$ near collapse. Thus, the relative variation in h may be decreased considerably by sacrificing a small fraction of the bias margin. The relative smallness of this variation in h is particularly important if half-bubbles on the lower platelet surface are to be propagated by permalloy circuits at the upper surface, as it is to be expected that there is an optimum circuit-domain separation for half-bubbles much as there is for standard cylindrical domains.[9]

In conclusion, we have shown that the half-bubble has a number of properties which are attractive for device applications. Its stability in the absence of external biasing represents a considerable advantage over the externally biased standard cylindrical domain. While some complexity is added by the requirement of gradient materials, the materials problem is simplified on another front by the fact that material thickness is unimportant for half-bubbles. Indeed, the half-bubble stabilizes on only one surface; if propagated from the same surface, irregularities in the second surface are of no consequence. These attractive properties of the half-bubble and its possible utility in avoiding the undesirable properties of hard-bubbles may more than compensate for the added difficulty in growing half-bubble materials.

VI. ACKNOWLEDGMENTS

The author is indebted to A. H. Bobeck, whose experiments provided the inspiration for this work. It is a pleasure to acknowledge many helpful conversations with and suggestions from F. B. Hagedorn and A. A. Thiele.

APPENDIX A

Magnetostatic Energy Invariance

Demagnetization fields equivalent to those of the standard cylindrical domain may be conceptually created through the use of two neutral subsystems of charges. The first consists of two parallel planes with magnetostatic charge density $\pm M_s$ and the second consists of two disks with charge density $\mp 2M_s$ placed on a common axis just inside

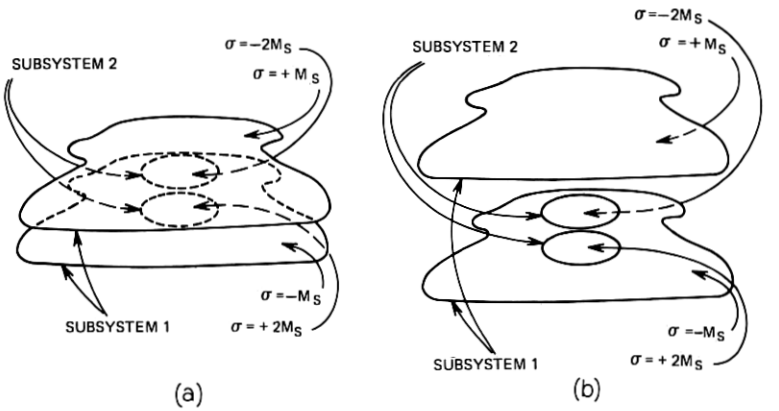

Fig. 6—Source-charge distribution for the demagnetization field of: (a) The standard cylindrical domain. (b) The half-bubble model.

the first subsystem (Fig. 6a). The distances between the upper plane and the upper disk, and between the lower plane and the lower disk are allowed to approach zero. The demagnetization field of the cylindrical domain is the superposition of the fields of the two isolated subsystems:

$$\vec{H}_d = \vec{H}_{d1} + \vec{H}_{d2} \,. \tag{47}$$

The magnetostatic energy of the domain (*including* the energy of the uniformly magnetized platelet) is the sum of the self-energies of subsystems 1 and 2 and their mutual interaction energy:

$$E_M = \frac{1}{8\pi} \int H_d^2 \, dV \tag{48a}$$

$$= \frac{1}{8\pi} \int H_{d1}^2 \, dV + \frac{1}{8\pi} \int H_{d2}^2 \, dV + \frac{1}{4\pi} \int \vec{H}_{d1} \cdot \vec{H}_{d2} \, dV. \tag{48b}$$

The transition from the magnetostatic field configuration of the standard cylindrical domain to that of the half-bubble model is achieved by moving the upper plane of charge upward (Fig. 6b). The field strength of subsystem one is unaltered by this change, while the self-energy of the subsystem increases linearly with the distance moved. The self-energy of subsystem two is, of course, unchanged, but remarkably the mutual interaction energy of the two subsystems is unchanged also. The latter invariance follows from the invariance of the field strength of subsystem

one and of the charge-neutrality of subsystem two (so that all field lines originating in the isolated subsystem two also terminate there). From these two properties it is easily seen that any lines of $\vec{H}_{d2}$ extending above the upper disk give a zero contribution to the mutual interaction energy of the two subsystems. If we now observe that the magnetostatic energy of introducing a domain into a uniformly magnetized platelet is just the sum of the self-energy of subsystem two and the mutual interaction energy, we see that this differential magnetostatic energy is independent of the position of the upper surface of the platelet (provided only that the domain remains inside of the platelet).

It is easily seen that this proof may be generalized to the cases in which M_s is a function of z or in which the domain assumes a more general form.

APPENDIX B

Energy of Half-Bubble Under Elliptical Distortions

The condition $(\partial E_T/\partial r_2)_{r_2=0} = 0$ in the absence of in-plane anisotropy is satisfied not only by our simple half-bubble model but by any convex domain having radial symmetry at equilibrium. For example, consider the generalized half-bubble shape

$$r_b(\varphi, z) = r_o(z) + r_2(z) \cos 2\varphi \tag{49}$$

where $r_2(z) \ll r_o(z)$ and $r_o(h) = 0$ (i.e., the half-bubble is closed at the top).

If there is no in-plane anisotropy, then

$$E_T(r_2) = E_T(-r_2) \tag{50}$$

since the shape function $r_b(\varphi, z) = r_o(z) - r_2(z) \cos 2\varphi$ transforms into that of eq. (49) under rotation. From eq. (50) it follows that

$$\left(\frac{\partial E_T}{\partial r_2}\right)_{r_2=0} \equiv 0. \tag{51}$$

Consequently, cross-derivatives such as $(\partial^2 E_T/\partial r_2\ \partial h)_{r_2=0}$ are also zero for the general domain shape given in eq. (49).

REFERENCES

1. Bobeck, A. H., private communication.
2. Bobeck, A. H., Blank, S. L., and Levinstein, H. J., "Multilayer Epitaxial Garnet Films for Magnetic Bubble Devices—Hard Bubble Suppression," B.S.T.J., *51*, No. 6 (July–August 1972), pp. 1431–1435.

3. Thiele, A. A., "The Theory of Cylindrical Magnetic Domains," B.S.T.J., *48*, No. 10 (December 1969), pp. 3287–3335.
4. Thiele, A. A., Bobeck, A. H., Della Torre, E., and Gianola, U. F., "The Energy and General Translation Force of Cylindrical Magnetic Domains," B.S.T.J., *50*, No. 3 (March 1971) pp. 711–773.
5. Liu, T. W., Bobeck, A. H., Nesbitt, E. A., Sherwood, R. C., and Bacon, D. D., J. Appl. Phys. *42*, (1971), p. 1641.
6. Hagedorn, F. B., private communication.
7. The factorization involving $l/h < 0$ is of no physical significance.
8. The half-bubble stability problem is closely related to the stability problem for the standard cylindrical domain in a platelet with gradients in M_s and σ_w normal to the platelet surface, the latter structure being essentially a half-bubble that has undergone run-through. The properties of this degenerate half-bubble are currently under investigation and will be reported in a separate paper.
9. Chen, Y. S., and Nelson, T. J., unpublished work.